

$L_4Fe_2As_2Te_{1-x}O_{4-y}F_y$ ($L = Pr, Sm, Gd$): a layered oxypnictide superconductor with T_c up to 45 K

S. Katrych¹, A. Pisoni¹, S. Bosma², S. Weyeneth², N. D. Zhigadlo³, R. Gaal¹,
J. Karpinski^{1,3}, L. Forró¹

¹*Institute of Condensed Matter Physics, EPFL, CH-1015 Lausanne, Switzerland*

²*Physik-Institut der Universität Zürich, Winterthurerstrasse 190, CH-8057 Zürich, Switzerland*

³*Laboratory for Solid State Physics, ETH Zurich, CH-8093 Zurich, Switzerland*

Abstract

The synthesis, structural and physical properties of iron lanthanide oxypnictide superconductors, $L_4Fe_2As_2Te_{1-x}O_4$ ($L = Pr, Sm, Gd$), with transition temperature at ~ 25 K are reported. Single crystals have been grown at high pressure using cubic anvil technique. The crystal structure consists of layers of L_2O_2 tetrahedra separated by alternating layers of chains of Te and of Fe_2As_2 tetrahedra: $-L_2O_2-Te-L_2O_2-Fe_2As_2-L_2O_2-Te-L_2O_2-$ (space group: $I4/mmm$, $a \sim 4.0$, $c \sim 29.6$ Å). Substitution of oxygen by fluorine increases the critical temperature, e.g. in $Gd_4Fe_2As_2Te_{1-x}O_{4-y}F_y$ up to 45 K. Magnetic torque measurements reveal an anisotropy of the penetration depths of ~ 31 .

PACS number(s): 81.10.-h, 74.62.Bf, 74.70.Xa, 74.25.-q

I. INTRODUCTION

The discovery of high temperature superconductivity in $LaFeAsO_{1-x}F_x$ ¹ has spiralled up an investigation of a variety of compounds consisting of M_2As_2 (M is a transition metal) layers alternating with L_2O_2 (L is a lanthanide metal) layers or metal layers (eg. Ba, Li or other). In the view of the fact that all of these compounds were reported already before discovery of superconductivity in $La1111$ ^{2, 3} and their synthesis procedure, as well as structure details were well investigated, great progress in finding of several new iron based superconductors was achieved by doping of known layered pnictide and oxypnictide in a less than one year. Superconductivity was also found in FeSe or “11” ($T_c = 8$ K)^{4, 5}, $Ba_{1-x}K_xFe_2As_2$ or “122” ($T_c = 38$ K)^{6, 7}, $LiFeAs$ or “111” ($T_c = 18$ K)^{8, 9}, $La_3Ni_4P_4O_2$ or “3442” ($T_c = 2.2$ K)^{10, 11}.

In this work we present the systematic study of superconducting compounds $L_4Fe_2As_2Te_{1-x}O_4$ ($L = Pr, Sm, Gd$) with a hitherto unknown structure. Our recent work¹², where crystal growth, structure and physical properties of an oxypnictide superconductor $Pr_4Fe_2As_2Te_{1-x}O_4$ with a critical temperature (T_c) close to 25 K were reported, triggered this study with the intention of increasing T_c of this compound.

The structure of $Pr_4Fe_2As_2Te_{1-x}O_4$ (also called 42214) reveals the same structural blocks as $PrFeAsO$ (1111) oxypnictide superconductor³: fluorite-type Pr_2O_2 layers alternating with anti-

fluorite-type Fe_2As_2 layers with a difference in a presence of intercalated Te atoms (Fig. 1a-c). Both structures are tetragonal with the space group $I4/mmm$ for the former and $P4/nmm$ for the latter.

For the 1111 phase two parameters are known how to increase T_c by modifying the structure or composition. One of them is pnictogen height h_P (half of the thickness of the Fe_2As_2 or S_2 , Fig. 1a-c), which as indicator for highest possible T_c should be close to $1.38 \text{ \AA}^{13,14}$. The LFeAsO for $L = \text{Sm}$ and Gd have h_P value close to the “optimal” one.

The other factor is doping. The pure stoichiometric, undoped 1111 phase does not reveal superconductivity¹. The most effective doping that results in T_c above 50 K is at the oxygen sites either by fluorine, hydrogen or by oxygen vacancies^{1, 15, 16}. Substitution of Sm by Th also leads to T_c above 50 K^{17, 18}.

According to our recent investigations^{12, 19} the lattice constant a , b , Fe_2As_2 layer thickness S_2 and $\text{Fe}_2\text{As}_2\text{-L}_2\text{O}_2$ interlayer distance S_3 are almost equal for both PrFeAsO and for $\text{Pr}_4\text{Fe}_2\text{As}_2\text{Te}_{1-x}\text{O}_4$ (Fig. 1a-c). In analogy to 1111 one can expect that “optimal” h_P and proper doping should lead to high T_c in 42214 compounds. $\text{L}_4\text{Fe}_2\text{As}_2\text{Te}_{1-x}\text{O}_4$ ($L = \text{Sm}$ and Gd) doped with fluorine, as one of the options, was assumed as the ideal candidate for increasing T_c in 42214 because h_P of LFeAsO ($L = \text{Sm}, \text{Gd}$) corresponds to the maximal T_c . To prove this suggestion a detailed structural study of undoped $\text{L}_4\text{Fe}_2\text{As}_2\text{Te}_{1-x}\text{O}_4$ ($L = \text{Pr}, \text{Sm}, \text{Gd}$) was preformed as well as the influence of fluorine substitution for oxygen on T_c in $\text{L}_4\text{Fe}_2\text{As}_2\text{Te}_{1-x}\text{O}_4$ ($L = \text{Sm}, \text{Gd}$) was studied.

Here we report high pressure crystal growth, structure and doping of $\text{L}_4\text{Fe}_2\text{As}_2\text{Te}_{1-x}\text{O}_{4-y}\text{F}_y$ ($L = \text{Pr}, \text{Sm}, \text{Gd}$) single crystals. The critical temperature of $\text{Gd}_4\text{2214}$ single crystals increased after F doping from 25 K up to 45 K.

II. EXPERIMENTAL DETAILS

The crystals of the $\text{Pr}_4\text{Fe}_2\text{As}_2\text{Te}_{1-x}\text{O}_4$, $\text{Sm}_4\text{Fe}_2\text{As}_2\text{Te}_{1-x}\text{O}_{4-y}\text{F}_y$ and $\text{Gd}_4\text{Fe}_2\text{As}_2\text{Te}_{1-x}\text{O}_{4-y}\text{F}_y$ were grown at high pressure from precursors (pre-sintered mixture of $0.9\text{PrAs} + 0.1\text{PrTe} + \text{FeO}$, $0.9\text{SmAs} + 0.1\text{TeO}_2 + 0.5\text{FeO} + 0.15\text{FeF}_2 + 0.35\text{Fe} + 0.1\text{Sm}$ and $\text{Fe} + 0.9\text{GdAs} + 0.1\text{GdTe} + 0.8\text{FeO} + 0.1\text{FeF}_2$, respectively) in NaCl/KCl flux. The procedure is described by Katrych *et al.*¹² The same procedure was used for the growth of $\text{L}_4\text{Fe}_2\text{As}_2\text{Te}_{1-x}\text{O}_4$ ($L = \text{Sm}, \text{Gd}$) crystals from stoichiometric mixture of high purity ($\geq 99.95\%$) L , LAs , FeO and TeO_2 .

The single crystals were studied on a 3 circle x-ray diffractometer equipped with a CCD detector (Bruker AXS Inc.). Data reduction and multi-scan absorption correction were performed using

the APEX2²⁰ and SAINT²¹ software. The crystal structure was solved by a direct method and full data set refined on F^2 , employing the programs SHELXS-97²² and SHELXL-97²³.

The magnetization as a function of temperature has been measured for individual single crystals of $L_4Fe_2As_2Te_{1-x}O_4$ ($L = Pr, Gd$) and $L_4Fe_2As_2Te_{1-x}O_{4-y}F_y$ ($L = Sm, Gd$) doped with fluorine. These experiments have been done with an MPMS with enhanced sensitivity (MPMS-XL).

Because individual $Sm_4Fe_2As_2Te_{1-x}O_4$ single crystals were too small, the magnetic susceptibility (M/H) measurement was performed on a powdered sample using a magnetic property measurement system (MPMS: Quantum Design) under zero-field-cooling (ZFC) and field-cooling (FC) conditions.

The electrical resistivity (ρ) of a $Sm_4Fe_2As_2Te_{1-x}O_{4-y}F_y$ single crystal was measured as a function of temperature using a standard four-probe method. Gold wires of 12 μm diameter were glued with silver paint on a 150 μm long sample in a van der Pauw geometry. The contact resistance was less than 200 Ω . A sensing current of 100 μA was generated using a Keithley 220 programmable current source and the resulting signal was measured by a Keithley 2182 nanovoltmeter. The sample was cooled in liquid helium bath cryostat from room temperature at a rate of 0.5 K/min.

The magnetic anisotropy measurements were carried out with a homemade magnetic torque sensor²⁴. A tiny $Sm_4Fe_2As_2Te_{1-x}O_{4-y}F_y$ single crystal ($\sim 100 \times 100 \times 10 \mu m^3$) was fixed on a platform hanging on piezoresistive legs. When a static magnetic field was applied to this anisotropic superconductor, a torque proportional to the vector product of magnetization and field appears and bends the piezoresistive legs. The resulting change in resistance can be read out electronically, yielding a signal proportional to the torque²⁴.

III RESULTS AND DISCUSSION

A. Structure analysis

The crystals of $Pr_4Fe_2As_2Te_{1-x}O_4$ with plate-like shape reveal nice quality with a mosaic spread of $\sim 1.1^\circ$ (Fig. 2).

Structure of 42214 (Fig. 1(a)) was determined and refined on the base of 670 independent reflections. Since the displacement parameter of Te was larger than that of others atoms, the occupation parameter for it was set as a free variable. Finally Te site reveals about 10 % of vacancies¹². The same Te deficiency was found in $L_4Fe_2As_2Te_{1-x}O_4$ ($L = Sm, Gd$) which was

refined using the $\text{Pr}_4\text{Fe}_2\text{As}_2\text{Te}_{1-x}\text{O}_4$ structural model. Table 1 and table 2 provide the results of structure determination and refinement.

Despite the entirely different stoichiometric composition or formula type, the determined structure has some resemblance to that of $\text{La}_3\text{Cu}_4\text{P}_4\text{O}_2$ ¹⁰ or another representative of its structure type, superconducting $\text{La}_3\text{Ni}_4\text{P}_4\text{O}_2$ (3442)¹¹. The number of atoms in the unit cells as well as the space group are the same (Pearson symbol: $tI26$, space-group: $I4/mmm$). Like in the 3442 the structure of 42214 consists of stacked fluorite-type L_2O_2 and anti-fluorite-type M_2Pn_2 layers. However, the sequence and numbers of 2 types of layers are dissimilar for the two structures, furthermore the atom in the centre of unit cell has positive charge $\text{L}^{\delta+}$ for 3442 and negative $\text{Te}^{\delta-}$ for 42214. The two structures are isoconfigurational and have interchanged corresponding structure motifs: $(\text{L}_2\text{O}_2)_2(\text{M}_2\text{Pn}_2)\text{Te}$ vs. $(\text{L}_2\text{O}_2)(\text{M}_2\text{Pn}_2)_2\text{L}$ (Fig. 1a-e), where $\text{L} = \text{Pr}, \text{Sm}, \text{Gd}$ and $\text{M} = \text{Fe}; \text{Pn} = \text{As}$ for the former and $\text{L} = \text{La}, \text{Ce}, \text{Nd}; \text{M} = \text{Cu}, \text{Ni}; \text{Pn} = \text{P}$ for the latter. Regarding the definition of Lima-de-Faria *et al*²⁵, the 42214 structure could be considered as an *anti* - $\text{La}_3\text{Cu}_4\text{P}_4\text{O}_2$ – crystal structure.

The 3442 phase is considered as an ordered mixture of LMPnO and LM_2Pn_2 ¹¹ (Fig.2c-d). The 42214 could be described as stacking of the 1111 with $\text{L}_2\text{O}_2\text{Te}$ ²⁶ (Fig. 1a-b-c).

Across the lanthanide series with increasing the number of atom in periodic table and decreasing of its covalent radius lattice constants, thickness of Pr_2O_2 layers S_1 decreases while thickness of Fe_2As_2 layer, S_2 ($2 \times h_P$), increases (Fig. 3). The corresponding S_2 and S_3 are very close for both 1111 and 42214 structures¹⁹ (Tab. 1, Fig. 1a-c) while the L_2O_2 (S_1) layer is by 0.1 Å thicker in 1111. The h_P parameter increases monotonically from 1.332 to 1.366 Å and is getting, as it was expected, close to “optimal” value for $\text{Sm}_4\text{Fe}_2\text{As}_2\text{Te}_{1-x}\text{O}$ and $\text{Gd}_4\text{Fe}_2\text{As}_2\text{Te}_{1-x}\text{O}$ (1.352(3) and 1.366(3) Å, respectively).

The fluorine-doped crystals of $\text{Sm}_4\text{Fe}_2\text{As}_2\text{Te}_{1-x}\text{O}_{4-y}\text{F}_y$ and $\text{Gd}_4\text{Fe}_2\text{As}_2\text{Te}_{1-x}\text{O}_{4-y}\text{F}_y$ were also studied by single crystal x-ray diffraction. The results are shown in tables 3 and 4. In both cases the lattice parameter c is smaller than for samples without fluorine. For $\text{Sm}_4\text{Fe}_2\text{As}_2\text{Te}_{1-x}\text{O}_{4-y}\text{F}_y$ c is even much smaller that could be caused by a high concentration of tellurium deficiency (about 28 at. %). The lattice constants a and b for $\text{Gd}_4\text{Fe}_2\text{As}_2\text{Te}_{1-x}\text{O}_{4-y}\text{F}_y$ remain almost the same as for sample without fluorine. For $\text{Sm}_4\text{Fe}_2\text{As}_2\text{Te}_{1-x}\text{O}_{4-y}\text{F}_y$ a and b are slightly smaller in comparison to $\text{Sm}_4\text{Fe}_2\text{As}_2\text{Te}_{1-x}\text{O}_4$. It is rather difficult to find any correlation or exact influence of fluorine doping with the lattice geometry because of different concentration of vacancies in Te site for each sample as well as of difficulties with estimation of the real fluorine content.

B. Magnetic properties

a) Samples with Te deficiency

The temperature dependence of the magnetic moment for the $\text{Sm}_4\text{Fe}_2\text{As}_2\text{Te}_{1-x}\text{O}_4$ powdered sample ($m = 0.02$ g) and for two small individual single crystals of $\text{L}_4\text{Fe}_2\text{As}_2\text{Te}_{1-x}\text{O}_4$ ($L = \text{Pr}, \text{Gd}$) is shown in figures 4 and 5, respectively. The $M(T)$ measurements for single crystals have been performed in various magnetic fields parallel to the c -axis, for the zero-field-cooling (ZFC) and field-cooling (FC) states. The observed signal reveals bulk superconductivity¹². Magnetic measurements performed on $\text{Sm}_4\text{Fe}_2\text{As}_2\text{Te}_{1-x}\text{O}_4$ powdered sample at applied field of 0.5 mT showed the onset of superconducting transition at ~ 25 K with relatively small superconducting shielding fraction (9.4 %, see the ZFC curve in Fig. 4, the density of the compound was calculated to be 7.48 g/cm³). The powdered sample was not single phase.

The onset for $\text{Sm}_4\text{Fe}_2\text{As}_2\text{Te}_{1-x}\text{O}_4$ sample as well as for both single crystals of $\text{L}_4\text{Fe}_2\text{As}_2\text{Te}_{1-x}\text{O}_4$ ($L = \text{Pr}, \text{Gd}$) is estimated to be nearly the same, $T_c \sim 25$ K (Fig. 4-5). The omnipresent Te deficiency could be assumed as a doping causing superconductivity. The application of small magnetic fields above of 1 mT already lead to a drastic broadening of the transition width, indicative for a very small lower critical field, H_{c1} .

b) Samples with Te deficiency and doped with fluorine

In Fig. 6 the result of fluorine doping can be seen. Fig. 6(a) shows $M(T)$ for the zero-field-cooling (ZFC) and field-cooling (FC) states of single crystal of $\text{Sm}_4\text{Fe}_2\text{As}_2\text{Te}_{0.72(1)}\text{O}_{4-y}\text{F}_y$. After substituting nominally 30% of oxygen by fluorine T_c increased from 25 K of to 40 K. Fig. 6(b) shows $M(T)$ for a $\text{Gd}_4\text{Fe}_2\text{As}_2\text{Te}_{0.92(1)}\text{O}_{4-y}\text{F}_y$ single crystal. Here, substitution nominally 20% of oxygen by fluorine increased T_c up to 45 K. It is not clear if maximum T_c has been obtained. Doping dependence on T_c should be investigated in broader range of compositions.

C. Transport measurement

The onset superconducting critical temperature is 36 K for $\text{Sm}_4\text{Fe}_2\text{As}_2\text{Te}_{1-x}\text{O}_{4-y}\text{F}_y$ (Fig. 7). The ρ - T curve suggests that the sample is not optimally doped and that some inhomogeneity is present in the structure. This might explain the small upturn in ρ just above the superconducting transition.

D. Magnetic torque studies

Figure 8 shows the torque as a function of the angle θ between the applied magnetic field H and the crystallographic c -axis. When the field direction is swept clockwise (CW) and counterclockwise (CCW), a hysteresis between the CW and CCW torque curves appears. This is

due to the pinning of the vortices on crystal defects²⁷. The data shown here is the average of the CW and CCW curves.

The angular torque data are analyzed with the Kogan model²⁸, which allows to extract the anisotropy γ of the material. The anisotropy parameter γ is defined as λ_c/λ_{ab} , where λ_i is the magnetic field penetration depth for a field along the crystallographic i -axis. The fit is done assuming a Werthamer-Helfand-Hohenberg²⁹ dependence of the upper critical field, with a slope at T_c given in Ref.¹².

The fit results in a rather high anisotropy of 31, measured at 25 K. This anisotropy is one of the highest among the iron-based superconductor family, consistent with the large distance between the superconducting Fe₂As₂ layers in this material.

IV CONCLUSION

Single crystals of layered superconductors L₄Fe₂As₂Te_{1-x}O₄ (L = Pr, Sm, Gd; x ~ 0.1) were grown using high-pressure cubic anvil technique. The structure reveals the stacking of anti-fluorite-type M₂Pn₂ and fluorite-type L₂O₂ layers alternating with the chain of tellurium atoms and could be considered as an *anti*-La₃Cu₄P₄O₂ – crystal structure. The critical temperature T_c is about 25 K and does not show any dependence on the kind of lanthanide atom.

Doping with fluorine increases T_c of Sm₄Fe₂As₂Te_{1-x}O_{4-y}F_y up to 40 K and of Gd₄Fe₂As₂Te_{1-x}O_{4-y}F_y up to 45 K. For determination of maximum T_c of 42214 more detailed studies of T_c dependence on doping is necessary.

This work was supported by the Swiss National Science Foundation (Project № 140760) and by the European Community FP7 Super-Iron Project.

* sergiy.katrych@epfl.ch

- ¹ Y. Kamihara, T. Watanabe, M. Hirano, and H. Hosono, J. Am. Chem. Soc. **130**, 3296 (2008).
- ² B. I. Zimmer, W. Jeitschko, J. r. H. Albering, R. Glaum, and M. Reehuis, J. Alloys Compd. **229**, 238 (1995).
- ³ P. Quebe, L. J. Terbüchte, and W. Jeitschko, J. Alloys Compd. **302**, 70 (2000).
- ⁴ G. Haegg and A. L. Kindstroem, Zeitschrift fuer Physikalische Chemie, Abteilung B: Chemie der Elementarprozesse, Aufbau der Materie **22**,, 453 (1933).
- ⁵ F.-C. Hsu, et al., Proceedings of the National Academy of Sciences **105**, 14262 (2008).
- ⁶ M. Pfisterer and G. Nagorsen, Z. Naturforsch. **B 35**, 703 (1980).
- ⁷ M. Rotter, M. Tegel, and D. Johrendt, Phys. Rev. Lett. **101**, 107006 (2008).
- ⁸ R. Juza and K. Langer, Zeitschrift für anorganische und allgemeine Chemie **361**, 58 (1968).

9 J. H. Tapp, Z. Tang, B. Lv, K. Sasmal, B. Lorenz, P. C. W. Chu, and A. M. Guloy, *Phys. Rev. B* **78**, 060505 (2008).

10 R. J. Cava, H. W. Zandbergen, J. J. Krajewski, T. Siegrist, H. Y. Hwang, and B. Batlogg, *Journal of Solid State Chemistry* **129**, 250 (1997).

11 T. Klimczuk, T. M. McQueen, A. J. Williams, Q. Huang, F. Ronning, E. D. Bauer, J. D. Thompson, M. A. Green, and R. J. Cava, *Phys. Rev. B* **79**, 012505 (2009).

12 S. Katrych, K. Rogacki, A. Pisoni, S. Bosma, S. Weyeneth, R. Gaal, N. D. Zhigadlo, J. Karpinski, and L. Forró, *Phys. Rev. B* **87**, 180508 (2013).

13 K. Kuroki, H. Usui, S. Onari, R. Arita, and H. Aoki, *Phys. Rev. B* **79**, 224511 (2009).

14 Y. Mizuguchi and et al., *Supercond. Sci. Technol.* **23**, 054013 (2010).

15 T. Hanna, Y. Muraba, S. Matsuishi, N. Igawa, K. Kodama, S.-i. Shamoto, and H. Hosono, *Phys. Rev. B* **84**, 024521 (2011).

16 K. Miyazawa, K. Kihou, P. M. Shirage, C.-H. Lee, H. Kito, H. Eisaki, and A. Iyo, *Journal of the Physical Society of Japan* **78**, 034712 (2009).

17 C. Wang and et al., *EPL (Europhysics Letters)* **83**, 67006 (2008).

18 N. D. Zhigadlo, S. Katrych, S. Weyeneth, R. Puzniak, P. J. W. Moll, Z. Bukowski, J. Karpinski, H. Keller, and B. Batlogg, *Phys. Rev. B* **82** (2010).

19 J. Karpinski, et al., *Physica C: Superconductivity* **469**, 370 (2009).

20 Computer code APEX2, version 2009.9 (Bruker AXS Inc., 2009).

21 Computer code SAINT, version 7.68A (Bruker AXS Inc., 2009).

22 G. Sheldrick, computer code SHELXS-97: Program for the Solution of Crystal Structures (University of Göttingen, Germany, 1997).

23 G. Sheldrick, computer code SHELXL-97: Program for the Refinement of Crystal Structures (University of Göttingen, Germany, 1997).

24 S. Kohout, J. Roos, and H. Keller, *Rev. Sci. Instrum* **78**, 013903 (2007).

25 J. Lima-de-Faria, E. Hellner, F. Liebau, E. Makovicky, and E. Parthe, *Acta Crystallographica Section A* **46**, 1 (1990).

26 F. A. Weber and T. Schleid, *Zeitschrift fuer Anorganische und Allgemeine Chemie* **625**, 1833 (1999).

27 M. Willemin, C. Rossel, J. Hofer, H. Keller, A. Erb, and E. Walker, *Phys. Rev. B* **58**, R5940 (1998).

28 V. G. Kogan, *Phys. Rev. B* **38**, 7049 (1988).

29 N. R. Werthamer, E. Helfand, and P. C. Hohenberg, *Physical Review* **147**, 295 (1966).

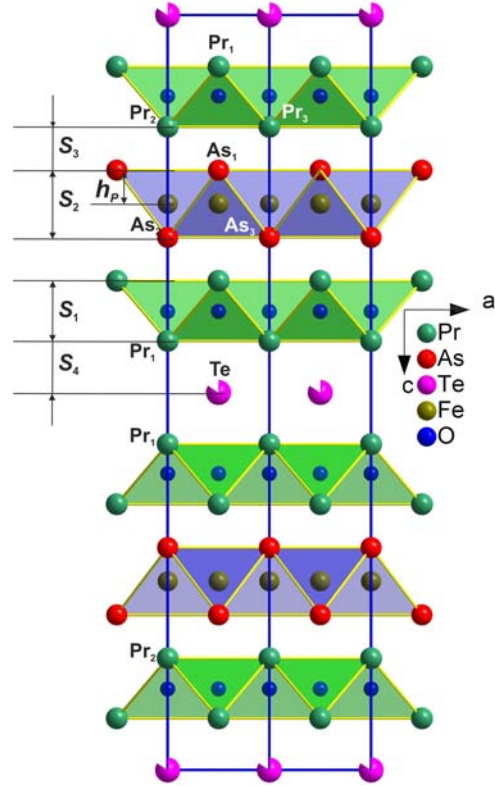
30 F. Nitsche, A. Jesche, E. Hieckmann, T. Doert, and M. Ruck, *Phys. Rev. B* **82**, 134514 (2010).

31 J. Yang, et al., *New J. Phys.* **11**, 025005 (2009).

32 T. C. Ozawa and S. M. Kauzlarich, *Science and Technology of Advanced Materials* **9**, 033003 (2008).

33 D. C. Johnston, *Advances in Physics* **59**, 803 (2010).

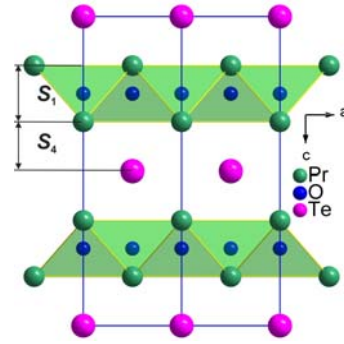
$L_4M_2Pn_2TeO_4$, L=Pr, Sm, Gd; M=Fe; Pn=As



(a)

$S_1=2.377(4)$ Å
 $1/2S_2=h_{Pr}=1.332(3)$
 $S_3=1.714(4)$
 $S_4=2.042(3)$
 Space group (SG): $I4/mmm$
 Pearson symbol (PS): $tI26$
 Lattice constants (LC): $a\sim 4.01$;
 $c\sim 29.86$ Å

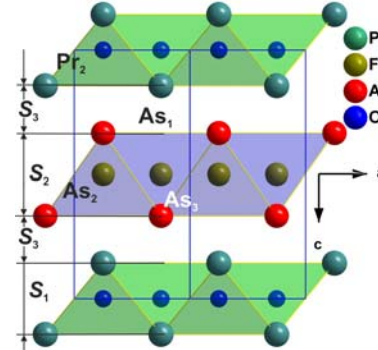
L_2O_2Te ; L=La-Nd,
 Sm-Ho²⁶



(b)

$S_1=2.339$ Å
 $S_4=2.045$
 SG: $I4/mmm$
 PS: $tI10$
 LC: $a\sim 4.06$;
 $c\sim 12.86$ Å

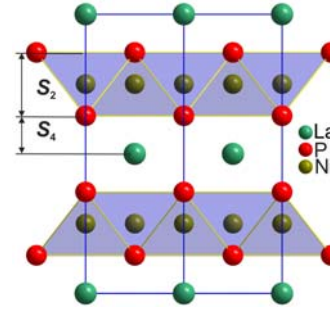
LMPnO; L=La-Nd, Sm,
 Gd-Ho^{16, 19, 30, 31}; M=Mn-Ni;
 Pn=P, As, Sb³²



(c)

$S_1=2.462(2)$ Å
 $1/2S_2=h_{Pr}=1.3429(9)$
 $S_3=1.716(1)$
 SG: $P4/nmm$
 PS: $tP8$
 LC: $a\sim 3.98$;
 $c\sim 8.58$ Å

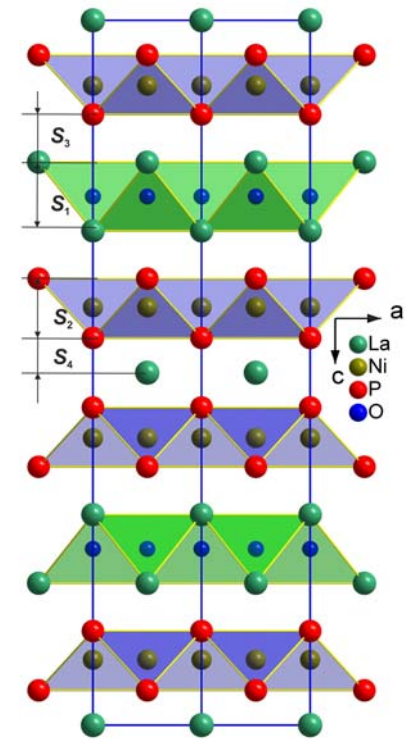
MeM_2Pn_2 ; Me=Ca, Sr, Ba, K,
 Eu, La, M=Cr-Cu, Ru, Rh, Ir
 Pn=P, As³³



(d)

$1/2S_2=h_{Pr}=1.21$ Å
 $S_4=1.19$
 SG: $I4/mmm$
 PS: $tI10$
 LC: $a\sim 4.01$;
 $c\sim 9.63$ Å

$L_3M_4Pn_4O_2$ L=La, Ce, Nd, M=Ni,
 Cu, Pn=P^{10, 11}



(e)

$S_1=2.550$ Å
 $S_2=2.200$
 $S_3=1.775$
 $S_4=1.291$
 SG: $I4/mmm$
 PS: $tI26$
 LC: $a\sim 4.01$;
 $c\sim 26.18$ Å

FIG. 1. (Color online) 1 x 2 unit cells projection in the ac plane (along b direction) from left to the right: (a) $L_4M_2Pn_2TeO_4$; (b) L_2O_2Te ; (c) LMPnO; (d) LM_2Pn_2 ; (e) $L_3M_4Pn_4O_2$.

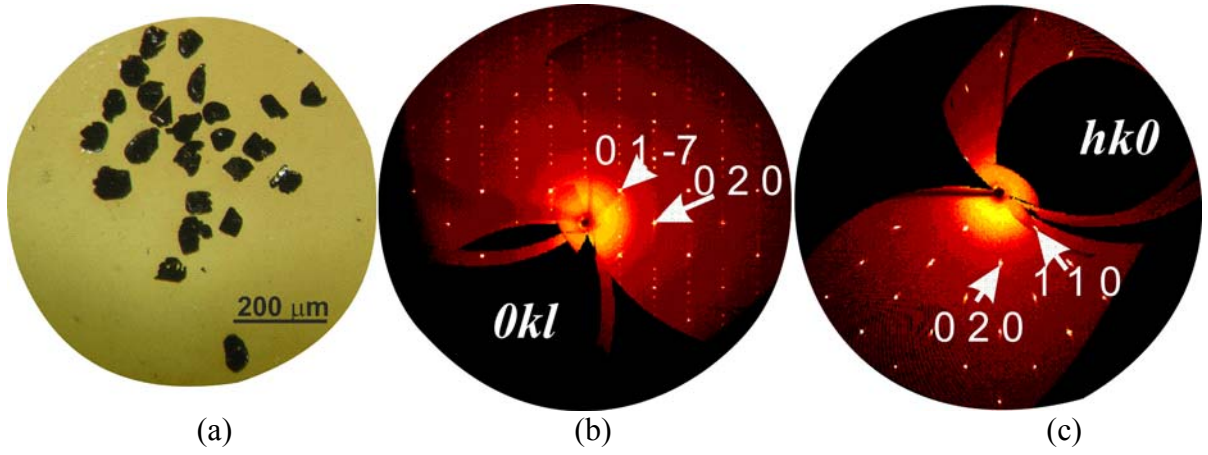


FIG. 2. (Color online) (a): single crystals of $\text{Pr}_4\text{Fe}_2\text{As}_2\text{Te}_{1-x}\text{O}_4$. (b) and (c): the reconstructed $(0kl)$ and $(hk0)$ reciprocal space sections for $\text{Pr}_4\text{Fe}_2\text{As}_2\text{Te}_{1-x}\text{O}_4$.

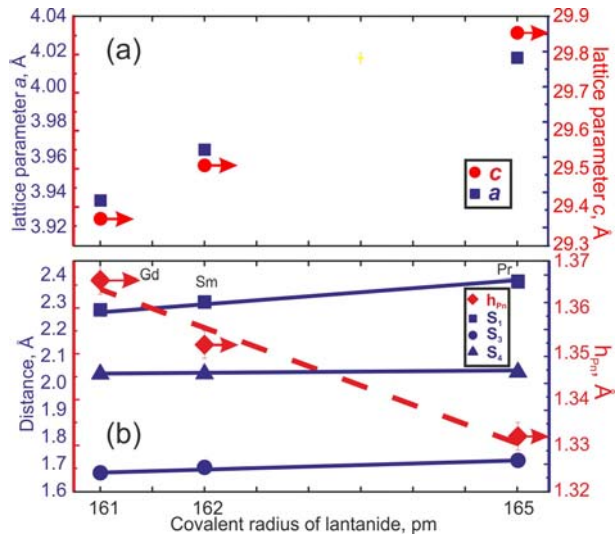


FIG. 3. (Color online) (a) and (b) - lattice parameters and layer thickness with interlayer distances as a function of covalent radius of lanthanide (arrows show that right Y axis should be used).

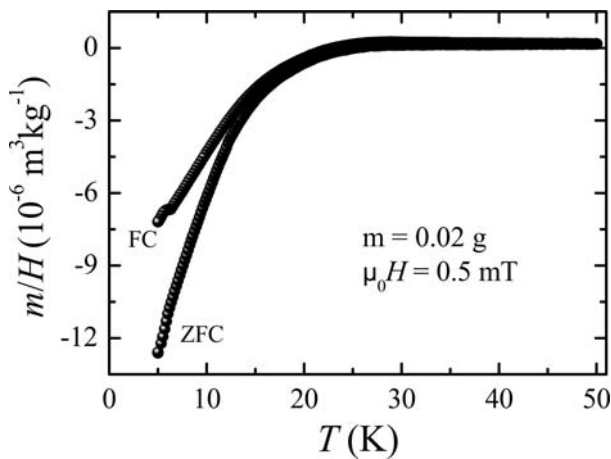


FIG. 4. Temperature dependence of the magnetic susceptibility for $\text{Sm}_4\text{Fe}_2\text{As}_2\text{Te}_{0.92(1)}\text{O}_4$ measured at 0.5 mT. FC is field cooled, ZFC is zero-field cooled.

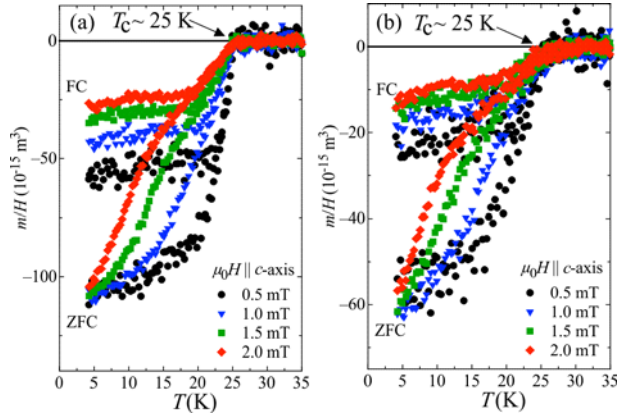


FIG. 5. (Color online) Temperature dependence of the magnetic susceptibility for:
a) $\text{Pr}_4\text{Fe}_2\text{As}_2\text{Te}_{0.88(1)}\text{O}_4$ and
b) $\text{Gd}_4\text{Fe}_2\text{As}_2\text{Te}_{0.90(1)}\text{O}_4$ single crystals.

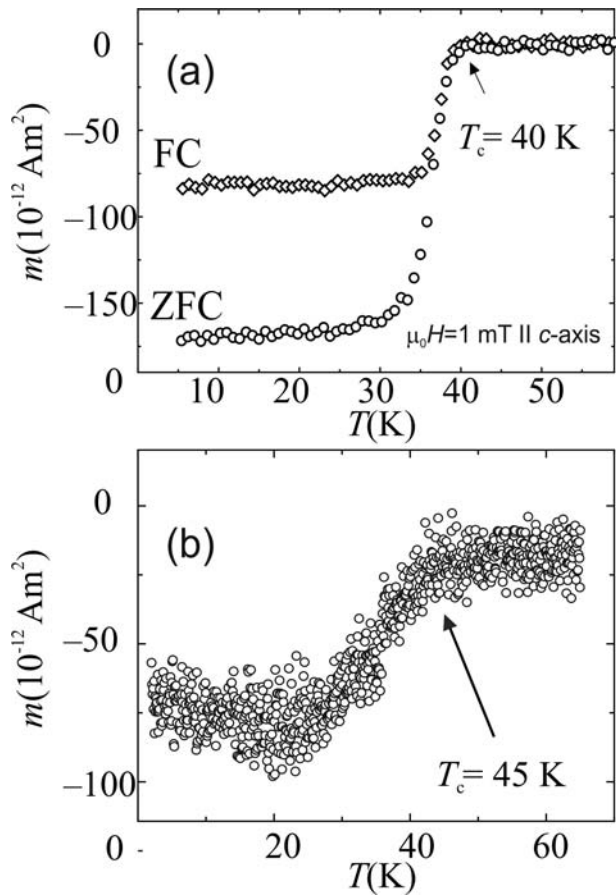


FIG. 6. Temperature dependence of the magnetization for:

- a) $\text{Sm}_4\text{Fe}_2\text{As}_2\text{Te}_{0.72(1)}\text{O}_{4-y}\text{F}_y$ and
 b) $\text{Gd}_4\text{Fe}_2\text{As}_2\text{Te}_{0.92(1)}\text{O}_{4-y}\text{F}_y$ single crystals.

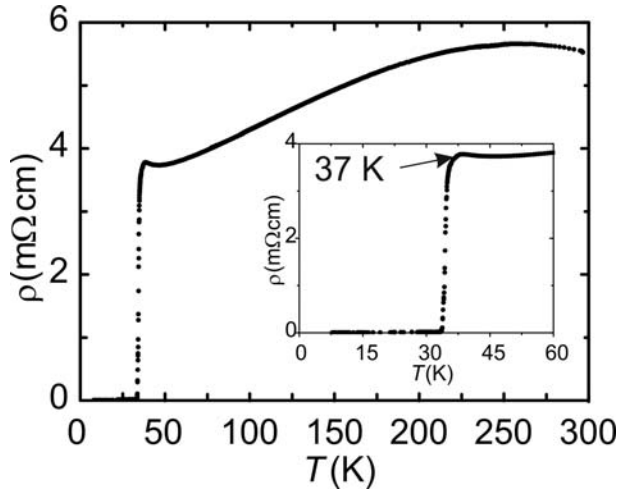


FIG. 7. Temperature dependence of the electrical resistivity for $\text{Sm}_4\text{Fe}_2\text{As}_2\text{Te}_{1-x}\text{O}_{4-y}\text{F}_y$ single crystal. Inset shows $\rho(T)$ around the superconducting transition.

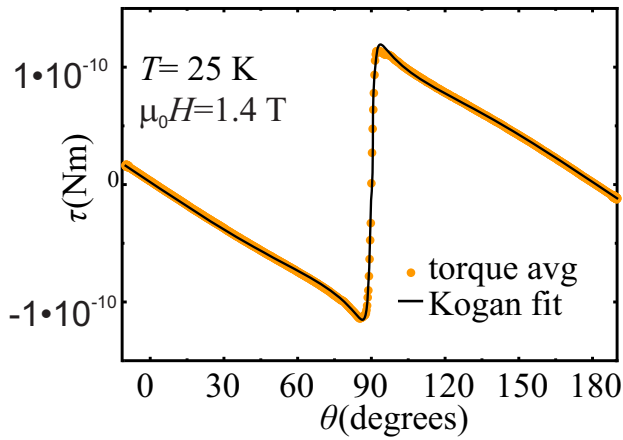


FIG. 8. (Color online) Torque as a function of the angle θ between the applied magnetic field H and the crystallographic c -axis of a single crystal of $\text{Sm}_4\text{Fe}_2\text{As}_2\text{Te}_{0.72(1)}\text{O}_{4-y}\text{F}_y$ at $T = 25$ K and $\mu_0 H = 1.4$ T. The solid line denotes a fit according to the Kogan model from which the anisotropy parameter $\gamma = 31$ was extracted.

TABLE 1. Details of the structure refinement for the $L_4Fe_2As_2Te_{1-x}O_4$ ($L = Pr, Sm, Gd$) crystals. The diffraction study is performed at 295(2) K using Mo K_{α} radiation with $\lambda = 0.71073 \text{ \AA}$. The lattice is tetragonal, space group is $I4/mmm$, $Z = 2$. A full-matrix least-squares method was employed to optimize F^2 .

Empirical formula	$Pr_4Fe_2As_2Te_{0.88(1)}O_4$	$Sm_4Fe_2As_2Te_{0.92(1)}O_4$	$Gd_4Fe_2As_2Te_{0.90(1)}O_4$
T_c, K	25	25	25
Unit cell dimensions, \AA	$a = 4.0165(2), c = 29.8572(16)$	$a = 3.9642(3), c = 29.509(2)$	$a = 3.9353(3), c = 29.369(3)$
Volume, \AA^3	481.66(4)	463.74(6)	454.82(7)
L_1 - L_2 , \AA	3.7026(6)	3.6278(4)	3.5928(8)
O-O=Fe-Fe, \AA	2.84009(14)	2.8031(2)	2.7827(2)
L_2 -As ₁ / L_1 -Te, \AA	3.3176(7)/3.4986(4)	3.2718(6)/3.4638(3)	3.2438(10)/3.4485(5)
L_2 -O/ L_1 -O, \AA	2.346(2)/2.320(3)	2.305(2)/2.2802(19)	2.284(4)/2.261(4)
As ₁ -As ₂ , \AA	3.8922(12)	3.8953(9)	3.8992(18)
Fe-As, \AA	2.4091(7)	2.3995(5)	2.3952(10)
As ₁ -Fe-As ₂ , β ($^\circ$)	107.77(2)	108.521(17)	108.97(3)
As ₂ -Fe-As ₃ , α ($^\circ$)	112.94(5)	111.39(4)	110.47(7)
S_1 , \AA	2.377(4)	2.302(4)	2.273(4)
$1/2S_2/h_P$, \AA	1.332(3)	1.352(3)	1.366(3)
S_3 , \AA	1.714(4)	1.688(4)	1.668(4)
S_4 , \AA	2.042(3)	2.036(3)	2.035(3)
Calculated density, g/cm^3	6.901	7.484	7.809
Absorption coefficient, mm^{-1}	32.145	37.855	41.860
$F(000)$	863	892	906
Crystal size, mm^3	0.11 x 0.07 x 0.03	0.11 x 0.06 x 0.03	0.11 x 0.08 x 0.03
Theta range for data collection, deg.	2.73 to 45.29	2.76 to 45.22	4.16 to 40.24
Index ranges	$-4 \leq h \leq 7, -7 \leq k \leq 8,$ $-47 \leq l \leq 59$	$-3 \leq h \leq 7, -6 \leq k \leq 7,$ $-58 \leq l \leq 57$	$-7 \leq h \leq 7, -7 \leq k \leq 4,$ $-41 \leq l \leq 52$
Reflections collected/unique	2778/670 $R_{\text{int}} = 0.0363$	3827/640 $R_{\text{int}} = 0.0410$	2986/490 $R_{\text{int}} = 0.0443$
Completeness to 2theta	98.4 %	97.3 %	97.8 %
Data/restraints/parameters	670/0/19	640/0/19	490/0/19
Goodness-of-fit on F^2	1.436	1.224	1.187
Final R indices [$> 2\sigma(I)$]	$R_1 = 0.0374, wR_2 = 0.0958$	$R_1 = 0.0298, wR_2 = 0.0679$	$R_1 = 0.0410, wR_2 = 0.0997$
R indices (all data)	$R_1 = 0.0406, wR_2 = 0.0997$	$R_1 = 0.0313, wR_2 = 0.0684$	$R_1 = 0.0428, wR_2 = 0.1002$

Fig. 1a

TABLE 2. Atomic coordinates and equivalent isotropic and anisotropic displacement parameters [$\text{\AA}^2 \times 10^3$] for the $L_4Fe_2As_2Te_{1-x}O_4$.

Atom	Site	x	y	z L=Pr/Sm/Gd	U_{iso}	$U_{11}=U_{22}$	U_{33}
L_1	4e	$1/2$	$1/2$	0.0684(1)/0.0690(1)/0.0693(1)	9(1)/7(1)/8(1)	8(1)/6(1)/6(1)	11(1)/8(1)/11(1)
L_2	4e	0	0	0.1480(1)/0.1470(1)/0.1467(1)	9(1)/7(1)/8(1)	9(1)/6(1)/7(1)	10(1)/8(1)/10(1)
As	4e	$1/2$	$1/2$	0.2054(1)/0.2042(1)/0.2035(1)	12(1)/9(1)/12(1)	13(1)/9(1)/13(1)	10(1)/8(1)/9(1)
Te	2a	0	0	0	16(1)/13(1)/17(1)	18(1)/15(1)/20(1)	12(1)/10(1)/12(1)
Fe	4d	$1/2$	0	$1/4$	11(1)/9(1)/10(1)	10(1)/8(1)/8(1)	12(1)/10(1)/13(1)
O	8g	$1/2$	0	0.1073(2)/0.1072(1)/0.1072(3)	10(1)/8(1)/8(1)	10(2)/6(1)/6(3)	12(2)/12(1)/15(3)

U_{iso} is defined as one third of the trace of the orthogonalized U_{ij} tensor. The anisotropic displacement factor exponent takes the form: $-2\pi^2 [(h^2 a^2 U_{11} + \dots + 2hka * b * U_{12})]$. For symmetry reasons $U_{23}=U_{13}=U_{12}=0$.

TABLE 3. Details of the structure refinement for the $L_4Fe_2As_2Te_{1-x}O_{4-y}F_y$ (L = Sm, Gd) crystals.

Empirical formula	$Sm_4Fe_2As_2Te_{0.72(1)}O_{4-y}F_y$	$Gd_4Fe_2As_2Te_{0.92(1)}O_{4-y}F_y$
T_c , K	40	45
Unit cell dimensions, Å, deg	$a= 3.9597(5)$, $c= 29.268(5)$	$a= 3.9363(6)$, $c= 29.350(5)$
Volume, Å ³	458.89(11)	454.77(12)
Ln_1 - Ln_2 , Å	3.6413(6)	3.6124(10)
O-O= Fe-Fe, Å	2.7999(4)	2.7834(4)
Ln_2 -As ₁ / Ln_1 -Te, Å	3.2424(8)/3.4406(5)	3.2271(13)/3.4454(7)
Ln_2 -O/ Ln_1 -O, Å	2.319(3)/2.275(3)	2.298(5)/2.263(5)
As ₁ -As ₂ , Å	3.8956(12)	3.9075(21)
Fe-As, Å	2.3987(7)	2.3987(12)
As ₁ -Fe-As ₂ , β (°)	108.59(2)	109.07(4)
As ₂ -Fe-As ₃ , α (°)	111.25(5)	110.27(8)
S_1 , Å	2.330(4)	2.301(4)
S_2/h_{pn} , Å	1.355(3)	/1.370(3)
S_3 , Å	1.633(4)	1.635(4)
S_4 , Å	1.999(4)	2.031(4)
Calculated density, g/cm ³	7.373	7.854
Absorption coefficient, mm ⁻¹	37.614	41.938
$F(000)$	871	910
Crystal size, mm ³	0.024 x 0.118 x 0.179	0.033 x 0.054 x 0.065
Theta range for data collection, deg.	2.78 to 32.49	4.17 to 36.21
Index ranges	-5=<h<=5, -5=<k<=5, -41=<l<=44	-4=<h<=6, -6=<k<=6, -42=<l<=48
Reflections collected/unique	2293/301 $R_{int}= 0.0559$	2294/390 $R_{int}= 0.0365$
Completeness to 2theta	97.7 %	97.5 %
Data/restraints/parameters	301/0/20	390/0/19
Goodness-of-fit on F^2	1.253	1.215
Final R indices [$I>2\sigma(I)$]	$R_1 = 0.0251$, $wR_2 = 0.0557$	$R_1 = 0.0422$, $wR_2 = 0.0982$
R indices (all data)	$R_1 = 0.0252$, $wR_2 = 0.0558$	$R_1 = 0.0433$, $wR_2 = 0.0987$

TABLE 4. Atomic coordinates and equivalent isotropic and anisotropic displacement parameters [$\text{Å}^2 \times 10^3$] for the $L_4Fe_2As_2Te_{1-x}O_{4-y}F_y$ (L = Sm, Gd) crystals.

Atom	Site	x	y	Z L = Sm/Gd	U_{iso}	$U_{11}=U_{22}$	U_{33}
L_1	4e	½	½	0.0683(1)/0.0692(1)	10(1)/8(1)	8(1)/6(1)	13(1)/11(1)
L_2	4e	0	0	0.1479(1)/0.1476(1)	10(1)/8(1)	8(1)/8(1)	12(1)/10(1)
As	4e	½	½	0.2037(1)/0.2033(1)	11(1)/11(1)	11(1)/13(1)	11(1)/8(1)
Te	2a	0	0	0	16(1)/15(1)	11(1)/17(1)	11(1)/11(1)
Fe	4d	½	0	¼	11(1)/10(1)	14(1)/9(1)	14(1)/12(1)
O	8g	½	0	0.1066(2)/0.1072(2)	9(1)/6(2)	7(2)/3(4)	16(1)/12(4)